Planned Trajectory Classification for Wheeled Mobile Robots to Prevent Rollover and Slip

Sang-Yun Jeon, Rakjoon Chung, and Dongjun Lee, *Member, IEEE*

***Abstract*—In this letter, a novel planned trajectory classification method (PTCM) is proposed to evaluate the safety of the car-like four-wheeled mobile robots (4-WMRs) with Ackermann steering and high-stiffness suspensions. To classify a planned trajectory to be safe or unsafe before the 4-WMR actually follows it, the conditions of the wheel forces (WFs: longitudinal, lateral, and normal forces for each wheel) necessary to execute the planned trajectory without rollover and slip are calculated using the passive decomposition of the WMR dynamics with the Pfaffian constraints of the no-rollover and no-slip conditions. Similar to the case of Navier's table problem, only nine-dimensional WFs projected onto the constrained space are identifiable among the twelve-dimensional WFs. This indeterminacy turns out not to affect the rollover prediction, yet does so for the slip prediction. For this, we propose novel optimistic and pessimistic methods, together upper and lower bounding the exact slip prediction. The proposed PTCM classifies the planned trajectory as safe if rollover and slip are not predicted and unsafe otherwise. The proposed PTCM is demonstrated and validated by simulations and outdoor experiments.**

***Index Terms*—Dynamics, robot safety, wheeled mobile robots.**

I. Introduction

WHEELED mobile robots (WMRs) are getting popular due to their high payload, energy efficiency, and ease of control and design. Especially, the market of the robotic logistics, delivery, and smart/intelligent transportation using the WMRs are growing exponentially [1] with the planning, control, and sensing technologies of WMRs quickly being matured [2], [3], [4]. Arguably, the most important issue for these applications with driverless WMRs, which may be catastrophic particularly during high-speed driving on inclined roads [5], [6], [7], [8].

Most of existing results for this adopt the real-time detection and control approach [5], [6], [7], that is, right after the rollover or slip is detected, the trajectory is modified, and the controller activated to mitigate the rollover and slip (e.g., loss of traction) while driving. During this process, the trajectory modification may cause time delay and preventing the rollover and slip of the WMRs by the controllers may not be possible due to the limit (or lack) of the actuation (e.g., friction cone constraint), all possibly compromising the safety of the WMRs. Therefore, a means to predict rollover and slip of the WMRs even before executing the planned trajectory can minimize the risk of the rollover and slip, thereby, substantially enhancing the operation safety of the WMRs.

In this letter, a novel planned trajectory classification method (PTCM) is proposed to classify the planned trajectories to be safe or unsafe before executing the trajectory by predicting rollover and slip for the car-like 4-WMRs with Ackermann steering and high-stiffness suspensions that are widely used in Robotics. For this, we first compute the desired state and its derivatives from the given planned trajectory. We then apply the passive decomposition [9], [10] to decompose the dynamics of the 4-WMR into the unconstrained (e.g., locked) and constrained (e.g., shape) dynamics under the Pfaffian constraints of the no-rollover and no-slip conditions. By utilizing the unconstrained dynamics, we can extract the input torques (e.g., controls) for the WMR to track the planned trajectory, whereas, by utilizing the constrained dynamics along with the input torques, we can obtain nine-dimensional wheel forces (WFs: longitudinal, lateral, and normal forces for each wheel) projected onto the constrained space to uphold the no-rollover and no-slip constraints during the planned trajectory tracking. Similar to the case of Navier's table problem or Painleve paradox, these WFs projected onto the constrained space only specify nine-dimensional information, yet, the unknowns are the twelve-dimensional WFs. This indeterminacy turns out not to affect the rollover prediction, yet, does so for the slip prediction.

To address this issue of indeterminacy, novel algorithms are proposed to predict the rollover and slip using the WFs projected onto the constrained space and their relations with the WFs instead of the twelve-dimensional WFs. The ZMP (zero-moment point) and friction cone model are, respectively, employed to propose the rollover and slip prediction algorithms as follows. First, as stated above, the ZMP can be calculated only with the WFs projected onto the constrained space, and the rollover can be predicted when the calculated ZMP is at the outside of the supporting polygon. Second, using the friction cone model, the slip is predicted if the required friction coefficient to prevent the slip is larger than the friction coefficient of the road. However, all the twelve-dimensional WFs are required to calculate the required friction coefficient of each wheel. Therefore, we

Manuscript received 8 January 2023; accepted 19 May 2023. Date of publication 1 June 2023; date of current version 8 June 2023. This letter was recommended for publication by Associate Editor U.-X. Tan and Editor L. Pallottino upon evaluation of the reviewers' comments. This work was supported in part by the Industrial Convergence Core Technology Development Program under Grant 10063172 funded by Ministry of Trade, Industry & Energy (MOTIE), Korea and in part by the Korea Institute for Advancement of Technology Grant funded by the MOTIE of Korea, through the HRD Program for Industrial Innovation under Grant P0020536. *(Corresponding author: Dongjun Lee.)*

Sang-Yun Jeon and Dongjun Lee are with the Department of Mechanical & Aerospace Engineering, Seoul National University and IAMD, Seoul 08826, Republic of Korea (e-mail: jeonsyun@snu.ac.kr; djlee@snu.ac.kr).

Rakjoon Chung is with the Department of Mechanical & Aerospace Engineering, Seoul National University and IAMD, Seoul 08826, Republic of Korea, and also with Robot Center, Samsung Research, Seoul 06765, Republic of Korea (e-mail: rock.chung@samsung.com).

This letter has supplementary downloadable material available at https://doi.org/10.1109/LRA.2023.3281936, provided by the authors.

Digital Object Identifier 10.1109/LRA.2023.3281936

propose two slip prediction algorithms using the relations between the WFs and the WFs projected onto the constrained space, one optimistic and the other pessimistic, which respectively predict the slip if a sufficient condition for the slip is satisfied and a sufficient condition for the no-slip is not satisfied (e.g., a necessary condition for the slip), together upper and lower bounding the exact slip prediction. For the slip prediction algorithms, high stiffness vertical suspensions are assumed to use the solution of the Navier's table problem [11] for the distribution of the vertical WFs.

The main contributions of this letter are as follows: (1) a novel planned trajectory classification method (PTCM) for 4-WMRs with Ackermann steering is proposed to predict the rollover and slip before the 4-WMRs actually follow the planned trajectories; (2) a novel way of calculating the conditions of the WFs required to prevent the rollover and slip is proposed, which is greatly facilitated by applying passive decomposition [9], [10]; and (3) the proposed PTCM is extensively validated by simulations and outdoor experiments, showing the promise of the proposed PTCM in practice.

The rest of this letter is organized as the follows. Related works are summarized in Section II. In Section III, the d'Alembert dynamics of the 4-WMR is formulated and decomposed into the constrained and unconstrained dynamics with the no-rollover and no-slip constraints. Using the desired state and decomposed dynamics, the input torques to follow the planned trajectory, the WFs projected onto the constrained space, and the relations between the WFs and the WFs projected onto the constrained space are calculated in Section IV. Section V provides the proposed rollover and slip prediction algorithms using the ZMP and friction cone model, and the PTCM is proposed using the rollover and slip prediction results. The proposed PTCM is verified by simulations and outdoor experiments in Section VI, and the conclusion of this letter is drawn in Section VII.

II. Related Works

Preventing rollover and slip before executing trajectories is an important and essential function for autonomous robots such as WMRs, humanoids, and quadruped robots. For the humanoids and quadruped robots, the trajectory planning with safety constraints (e.g., ZMP [12], [13], [14], friction cone constraints [12], and contact force constraints [15]) are widely used, yet few trajectory planning for WMRs and vehicles (e.g., [16]) consider the safety constraints. In [12], a spring-loaded inverted pendulum (SLIP) model is used for a two-legged robot to predict the vertical forces at the contact points, and the ZMP and friction cone constraints are founded as functions of the control inputs and the vertical forces, respectively. The ZMP for the legged and wheeled-legged quadruped robots can be, respectively, calculated using simplified models such as the cart-table [13], [17] and mass-less legs [14] models without using contact forces for the trajectory optimization. In [15], constrained forces to prevent the slip are predicted using the inverse dynamics of quadruped robots and orthogonal decomposition, and the control inputs are optimized to minimize the predicted constrained forces with contact force and bounded input constraints. However, the safety constraints used in [12], [13], [14], [15], [16] increase computational complexities of the trajectory planning.

For the computationally efficient rollover and slip prevention, we propose a novel PTCM for 4-WMRs with the Ackermann steering using the ZMP and friction cone model, and the major challenge of the proposed PTCM is identifying the twelve-dimensional WFs to calculate the ZMP and required friction coefficient. Unfortunately, it is turned out that we cannot identify all twelve-dimensional WFs for the 4-WMRs in SE(3), and the ZMP and required friction coefficient cannot be calculated using the twelve-dimensional WFs. The existing methods for humanoids and quadruped robots [12], [13], [14], [15], [17] cannot be directly applied for the 4-WMRs, because less than four contacts points, which do not cause the indeterminacy of the WFs for the 4-WMRs, are considered, and the simplified models for WMRs (e.g., planar [5], roll plane [6], [7], and double-track [16] models) are not proper for modeling 4-WMR motions in SE(3). Therefore, we propose novel rollover and slip prediction algorithms that calculate the ZMP and required friction coefficient using the identifiable nine-dimensional WFs projected onto the constrained space to uphold the no-rollover and no-slip constraints instead of the twelve-dimensional WFs.

To our best knowledge, this is the first time that a calculation method for the conditions of the WFs to prevent both rollover and slip is proposed using the 4-WMR dynamics in SE(3) and the indeterminacy of the calculation of the WFs required to follow a planned trajectory without both rollover and slip is theoretically analysed for the 4-WMRs. Moreover, the calculation of the conditions of the WFs is simplified by using the passive decomposition [9], [10] in this letter. The proposed PTCM can predict the rollover and slip without using sensor measurements or offline calibration, required in [5], [6], [7], [8], and also can be used for computationally efficient double-checks with existing real-time rollover and slip detection methods or safety checks of sampled trajectories for the model predictive controls (MPCs).

III. Decomposed Dynamics for 4-WMR

In this section, the d'Alembert dynamics with the no-rollover and no-slip constraints is formulated to express the movement of the 4-WMR. The no-rollover and no-slip constraints are formulated as the Pfaffian constraints, and the Pfaffian constraints are used to decompose the d'Alembert dynamics to simplify the calculation of the WFs and input torques which are used for the proposed rollover and slip prediction algorithms. The d'Alembert dynamics of the 4-WMR is derived in Section III-A, and the Pfaffian constraints are founded in Section III-B. In Section III-C, the d'Alembert dynamics is decomposed into the constrained and unconstrained dynamics using the passive decomposition [9], [10].

A. D'alembert Dynamics for 4-WMR

The configuration of the 4-WMR in Fig. 1 is defined as $q = \{g_{\mathcal{GB}}, \delta, \varphi_1, \varphi_2, \varphi_3, \varphi_4\}$ where $g_{\mathcal{GB}} \in \Re^{4\times4}$ is the homogeneous transformation matrix from the global frame $\{\mathcal{G}\}$ to the body frame $\{\mathcal{B}\}$, δ is the steering angle represented in the body frame $\{\mathcal{B}\}$, φ_i is the rotated angle of the i-th wheel represented in the i-th wheel frame $\{\mathcal{W}_i\}$, and the wheel index $i \in W = \{1, 2, 3, 4\}$. The quantities $T_{(\bullet)}$, $W_{(\circ)}$, and H are, respectively, the displacements between the sprung mass center O and each wheel center C_i along the x, y, and z-axes of $\{\mathcal{B}\}$

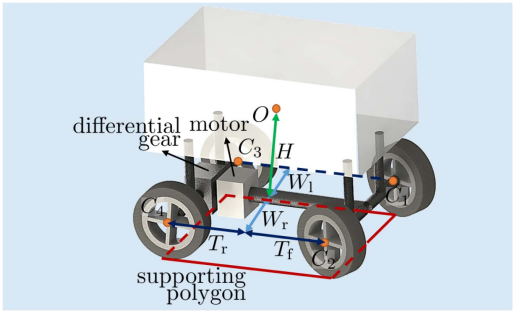

Fig. 1. Wheel configuration and supporting polygon of the 4-WMR.

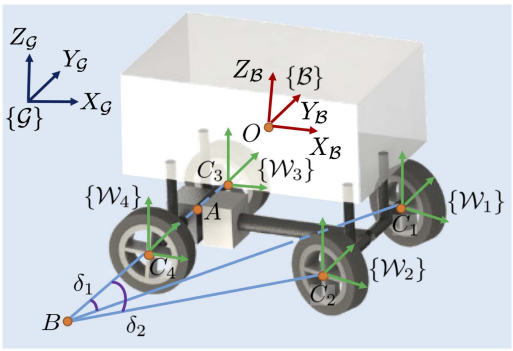

Fig. 2. Ackermann steering geometry and global, body, and wheel frames.

as shown in Fig. 1 where $(\bullet) \in \{\mathrm{f}, \mathrm{r}\}$ and $(\circ) \in \{\mathrm{l}, \mathrm{r}\}$. The front wheel steering angles δ_1 and δ_2 satisfy the Ackermann geometry $\cot(\delta_1) = \cot(\delta) - W_l/(T_f + T_r)$ and $\cot(\delta_2) = \cot(\delta) + W_r/(T_f + T_r)$ where $\tan(\delta) = (T_f + T_r)/L_{\mathrm{in}}$, $L_{\mathrm{in}} = (T_\mathrm{r} \cdot v_x + (H + r_w) \cdot v_z)/(\omega_z \cdot T_\mathrm{r} - \omega_x \cdot (H + r_w))$ is the distance between A (e.g., rear shaft center) and B (e.g., instantaneous center of rotation) in Fig. 2, r_w is the wheel radius, and the body linear and angular velocities represented in $\{\mathcal{B}\}$ are, respectively, $V_\mathcal{B} = [v_x\ v_y\ v_z]^\mathrm{T}$ and $\Omega_\mathcal{B} = [\omega_x\ \omega_y\ \omega_z]^\mathrm{T}$. It is assumed that the rear wheel steering angles $\delta_3 = \delta_4 = 0$ as typical 4-WMRs. The d'Alembert dynamics of the 4-WMR is then written by

$$M(q)\ddot{q} + C(q, \dot{q})\dot{q} + G(q) - J_f^\mathrm{T} \cdot f = \tau \tag{1}$$

where the velocity vector $\dot{q} = [V_\mathcal{B}^\mathrm{T}\ \Omega_\mathcal{B}^\mathrm{T}\ \dot{\delta}\ \dot{\varphi}_1\ \dot{\varphi}_2\ \dot{\varphi}_3\ \dot{\varphi}_4]^\mathrm{T} \in \Re^{11}$, the acceleration vector $\ddot{q}$ is the time derivative of $\dot{q}$ (e.g., $\ddot{q} = d\dot{q}/dt$), $M(q) \in \Re^{11\times11}$ is called the inertial matrix, $C(q, \dot{q}) \in \Re^{11\times11}$ is the Coriolis matrix, and $G(q) \in \Re^{11\times1}$ is the gravity matrix, the Jacobian matrix J_f is defined as

$$J_f = [J_{f,1}\ J_{f,2}\ \mathrm{O}_{12\times1}\ J_{f,3}]$$

$$J_{f,1} = [R_{\mathcal{B}\mathcal{W}_1}\ R_{\mathcal{B}\mathcal{W}_2}\ \mathrm{I}_{3\times3}\ \mathrm{I}_{3\times3}]^\mathrm{T}$$

$$J_{f,2} = [l_{OD_1} \times R_{\mathcal{B}\mathcal{W}_1}\ l_{OD_2} \times R_{\mathcal{B}\mathcal{W}_2}\ [l_{OD_3}\times]\ [l_{OD_4}\times]]^\mathrm{T}$$

$$J_{f,3} = \begin{bmatrix} -r_w & 0 & 0 & 0 & 0 & 0 & 0 & 0 & 0 & 0 & 0 & 0 \\ 0 & 0 & 0 & -r_w & 0 & 0 & 0 & 0 & 0 & 0 & 0 & 0 \\ 0 & 0 & 0 & 0 & 0 & 0 & -r_w & 0 & 0 & 0 & 0 & 0 \\ 0 & 0 & 0 & 0 & 0 & 0 & 0 & 0 & 0 & -r_w & 0 & 0 \end{bmatrix}^\mathrm{T} \tag{2}$$

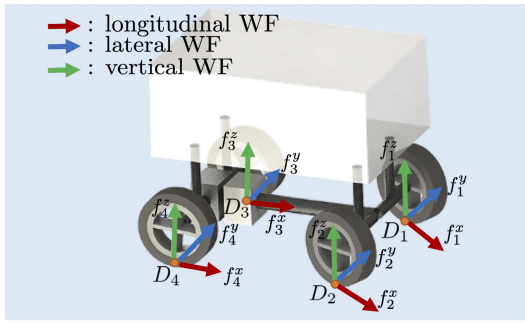

Fig. 3. Wheel forces (WFs) in SE(3) for each wheel.

the quantity f is a vector constructed with the twelve-dimensional WFs shown in Fig. 3, i.e., $f_i = [f_i^x\ f_i^y\ f_i^z]^\mathrm{T} \in \Re^3$, $R_{\natural\natural}$ is the rotation matrix defined to transform a vector in a frame $\{\natural\}$ to another frame $\{\sharp\}$, and $l_{\alpha\beta}$ is a vector from α to β represented in $\{\mathcal{B}\}$ where α and β are the points illustrated in Fig. 2 and Fig. 3. For the 4-WMR shown in Fig. 1, the input can be defined as $\tau = [\mathrm{O}_{1\times6}\ \tau_\delta\ 0\ 0\ \tau_\varphi\ \tau_\varphi]^\mathrm{T} \in \Re^{11}$ where τ_δ is the steering torque applied to the steering wheel, τ_φ is the rear wheel drive torque which is distributed by the differential gear, and $\mathrm{I}_{a\times b}$ and $\mathrm{O}_{a\times b}$ are, respectively, the identity and zero matrices of size $[a \times b]$.

B. Pfaffian Constraints

The no-rollover and no-slip constraints for the 4-WMR can be described as the following.

1) Each wheel does not slip in its longitudinal direction: $\dot{\varphi}_i = [1\ 0\ 0] \cdot R_{\mathcal{B}\mathcal{W}_i}^\mathrm{T} \cdot (V_\mathcal{B} + \Omega_\mathcal{B} \times l_{OD_i})/r_w$ for $^\forall i \in W$.
2) Each wheel does not slip in its lateral direction: $\tan(\delta) = (T_\mathrm{f} + T_\mathrm{r})/L_{\mathrm{in}}$ and $V_y^\mathcal{B} = \omega_z \cdot T_\mathrm{r} - \omega_x \cdot (H + r_w)$.
3) The 4-WMR does not move to the z-axis of $\{\mathcal{B}\}$: $\sum_{i\in W}[0\ 0\ 1] \cdot (V_\mathcal{B} + \Omega_\mathcal{B} \times l_{OC_i}) = 0$.
4) The angular velocities of the 4-WMR along the x and y-axes of $\{\mathcal{B}\}$ are zeros: $\omega_x = 0$ and $\omega_y = 0$.

The above no-rollover and no-slip constraints can be formulated as $\tilde{A}(q)\dot{q} = \mathrm{O}_{9\times1}$ where the matrix $\tilde{A}(q) \in \Re^{9\times11}$ is the Pfaffian constraint matrix with $\mathrm{rank}(\tilde{A}(q)) = 9$.

C. Decomposed Dynamics Using Passive Decomposition

To calculate the WFs that prevent the rollover and slip, the desired state and its derivatives (e.g., q, $\dot{q}$, and $\ddot{q}$) and the input torques τ to follow the planned trajectory are required as expressed in (1), and the desired state and its derivatives can be obtained from the planned trajectory. This section provides the decomposed dynamics of the 4-WMR into the constrained and unconstrained dynamics which is used to calculate τ and f in Sections IV-A and IV-B, respectively. The unconstrained dynamics, which is the projected dynamics onto the unconstrained space (e.g., null space of $\tilde{A}(q)$), simplifies the calculation of τ, because there is no WFs related term in the unconstrained dynamics, and τ can be directly calculated using the unconstrained dynamics as described in Section IV-A. In addition, the constrained dynamics, which is the projected dynamics onto the constrained space (e.g., row space of $\tilde{A}(q)$), can be used to calculate f by substituting the calculated τ as described in Section IV-B. To decompose the 4-WMR dynamics in (1) into

the constrained and unconstrained dynamics, the row and null space basis matrices of $\tilde{A}(q)$ (e.g., $\Delta_\perp$ and $\Delta_\top$, respectively) are defined as [9], [10]

$$\Delta_\perp = M^{-1}(q)\tilde{A}^{\mathrm{T}}(q)\left(\tilde{A}(q)M^{-1}(q)\tilde{A}^{\mathrm{T}}(q)\right)^{-1} \in \Re^{11\times 9}$$
$$\Delta_\top = \mathrm{null}(\tilde{A}(q)) \in \Re^{11\times 2}$$

and thanks to the properties of the above $\Delta_\perp$ and $\Delta_\top$ from the passive decomposition, i.e., $\tilde{A}(q)\Delta_\perp = \mathrm{I}_{9\times 9}$, $\tilde{A}(q)\Delta_\top = \mathrm{O}_{9\times 1}$, and $\Delta_\perp^{\mathrm{T}} M(q)\Delta_\top = \mathrm{O}_{9\times 2}$, the decomposed dynamics has advantage of simplicity [9], [10]. The notation $\mathrm{null}(K)$ represents the null space basis matrix of a matrix K, and we select

$$\Delta_\top = \frac{1}{\kappa_0}\cdot\begin{bmatrix} 0 & 0 & 0 & 0 & 0 & 0 & \kappa_0 & 0 & 0 & 0 & 0 \\ \kappa_1 & \kappa_2 & 0 & 0 & 0 & \kappa_3 & 0 & \kappa_4 & \kappa_5 & \kappa_6 & \kappa_7 \end{bmatrix}^{\mathrm{T}} \tag{3}$$

where

$$\kappa_0 = \kappa_6 + \kappa_7,\ \kappa_1 = r_w\cdot(T_f + T_r),\ \kappa_2 = r_w\cdot T_r\cdot\tan(\delta)$$
$$\kappa_3 = r_w\cdot\tan(\delta),\ \kappa_4 = (T_f + T_r)\cdot\tan(\delta)/\sin(\delta_1)$$
$$\kappa_5 = (T_f + T_r)\cdot\tan(\delta)/\sin(\delta_2),\ \kappa_6 = (T_f + T_r) - W_l\cdot\tan(\delta)$$
$$\kappa_7 = (T_f + T_r) + W_r\cdot\tan(\delta)$$

to simplify the projected input torque onto the unconstrained space as $\Delta_\top^{\mathrm{T}}\tau = [\tau_\delta\ \tau_\varphi]^{\mathrm{T}}$. The first column of $\Delta_\top$ is the basis vector related to the steering for the z-axis rotational movement in $\{\mathcal{B}\}$, and the last column of $\Delta_\top$ is the basis vector related to the wheel rotations for the x-axis translational movement in $\{\mathcal{B}\}$. The velocity vector $\dot{q}$ can be represented as [9], [10]

$$\dot{q} = S\nu \tag{4}$$

where $S = [\Delta_\top\quad \Delta_\perp]$, $\nu = [\nu_{\mathrm{L}}^{\mathrm{T}}\quad \nu_{\mathrm{E}}^{\mathrm{T}}]^{\mathrm{T}}$, and the vector $\nu_{\mathrm{L}} \in \Re^2$ and $\nu_{\mathrm{E}} \in \Re^9$ are the velocity vectors projected onto the unconstrained and constrained spaces, respectively. The acceleration vector $\ddot{q}$ is then written as [9], [10]

$$\ddot{q} = \dot{S}\nu + S\dot{\nu} \tag{5}$$

by differentiating $\dot{q}$ in (4). By multiplying $\Delta_\top^{\mathrm{T}}$ and $\Delta_\perp^{\mathrm{T}}$, respectively, to (1) and substituting $\dot{q}$, i.e., (4), and $\ddot{q}$, i.e., (5) into the multiplication results, the decomposed dynamics is derived as

$$\Delta_\top^{\mathrm{T}} M(q)\Delta_\top\dot{\nu}_{\mathrm{L}} + \Delta_\top^{\mathrm{T}}(M(q)\dot{S} + C(q,\dot{q})S)\nu + \Delta_\top^{\mathrm{T}} G(q) - \Delta_\top^{\mathrm{T}}\cdot J_f^{\mathrm{T}}\cdot f = \Delta_\top^{\mathrm{T}}\tau \tag{6}$$

$$\Delta_\perp^{\mathrm{T}} M(q)\Delta_\perp\dot{\nu}_{\mathrm{E}} + \Delta_\perp^{\mathrm{T}}(M(q)\dot{S} + C(q,\dot{q})S)\nu + \Delta_\perp^{\mathrm{T}} G(q) - \Delta_\perp^{\mathrm{T}}\cdot J_f^{\mathrm{T}}\cdot f = \Delta_\perp^{\mathrm{T}}\tau. \tag{7}$$

The equations (6) and (7) can be simplified by using the fact that $\nu_{\mathrm{E}} = \dot{\nu}_{\mathrm{E}} = \mathrm{O}_{9\times 1}$ if the Pfaffian constraints are satisfied, and $\Delta_\top^{\mathrm{T}}\cdot J_f^{\mathrm{T}} = \mathrm{O}_{2\times 12}$ by the definitions of J_f and $\Delta_\top$ in (2) and (3). Then, we have

$$\Delta_\top^{\mathrm{T}} M(q)\Delta_\top\dot{\nu}_{\mathrm{L}} + \Delta_\top^{\mathrm{T}}(M(q)\dot{\Delta}_\top + C(q,\dot{q})\Delta_\top)\nu_{\mathrm{L}} + \Delta_\top^{\mathrm{T}} G(q) = \Delta_\top^{\mathrm{T}}\tau \tag{8}$$

$$\Delta_\perp^{\mathrm{T}}(M(q)\dot{\Delta}_\top + C(q,\dot{q})\Delta_\top)\nu_{\mathrm{L}} + \Delta_\perp^{\mathrm{T}} G(q) - \Delta_\perp^{\mathrm{T}}\cdot J_f^{\mathrm{T}}\cdot f = \Delta_\perp^{\mathrm{T}}\tau. \tag{9}$$

The equations (8) and (9) express the unconstrained and constrained dynamics, respectively. The physical meaning of the decomposed dynamics is that the WFs projected onto the constrained space $\Delta_\perp^{\mathrm{T}}\cdot J_f^{\mathrm{T}}\cdot f$ should satisfy the constrained dynamics in (9) to prevent the rollover and slip, and the input projected onto the unconstrained space $\Delta_\top^{\mathrm{T}}\tau$ rotates the steering and wheel angles to generate the movement of the 4-WMR.

IV. Calculation of Forces and Torques

Using the decomposed dynamics in (8) and (9), τ and f are calculated in this section. The quantities τ, ν_{L}, and $\dot{\nu}_{\mathrm{L}}$ are the only unknowns in the unconstrained dynamics in (8), and ν_{L} and $\dot{\nu}_{\mathrm{L}}$ can be, respectively, calculated using the equation (4) and (5) with $\dot{q}$ and $\ddot{q}$ from the planned trajectory where $\nu_{\mathrm{E}} = \dot{\nu}_{\mathrm{E}} = \mathrm{O}_{9\times 1}$. The details for the calculation of τ, ν_{L}, and $\dot{\nu}_{\mathrm{L}}$ are provided in Section IV-A. In Section IV-B, the indeterminacy of the WFs f is discussed, and the projected WFs onto the constrained space λ, which are identifiable using the constrained dynamics in (9), are defined for the proposed rollover and slip prediction algorithms in Section V. The relations between f and λ to satisfy the no-rollover and no-slip constraints are also provided in Section IV-B, and these relations are used for the proposed slip prediction algorithms in Section V-B to resolve the indeterminacy of the WFs.

A. Calculation of Input Torques

When $\nu_{\mathrm{E}} = \mathrm{O}_{9\times 1}$ is substituted into (4), the relation between $\dot{q}$ and ν_{L} is expressed as

$$\dot{q} = \Delta_\top\cdot\nu_{\mathrm{L}}. \tag{10}$$

The matrix $\Delta_\top$ has the full-rank, because the columns in $\Delta_\top$ are the independent null space basis vectors of $\tilde{A}(q)$, and ν_{L} is calculated as $\nu_{\mathrm{L}} = (\Delta_\top^{\mathrm{T}}\Delta_\top)^{-1}\Delta_\top^{\mathrm{T}}\dot{q}$ using the equation (10). Similarly, $\dot{\nu}_{\mathrm{L}}$ can be obtained using (5) and $\nu_{\mathrm{E}} = \mathrm{O}_{9\times 1}$ as $\dot{\nu}_{\mathrm{L}} = (\Delta_\top^{\mathrm{T}}\Delta_\top)^{-1}\Delta_\top^{\mathrm{T}}(\ddot{q} - \dot{\Delta}_\top\nu_{\mathrm{L}})$. The input torques projected onto the unconstrained space $\Delta_\top^{\mathrm{T}}\tau = [\tau_\delta\ \ \tau_\varphi]^{\mathrm{T}}$ can be calculated using (8) with the known variables, i.e., q, $\dot{q}$, ν_{L}, and $\dot{\nu}_{\mathrm{L}}$. The calculated input torques in this section are used in Section IV-B.

B. Calculation of Wheel Forces and Indeterminacy

According to the constrained dynamics in (9), the WFs should satisfy the following equation to prevent the rollover and slip.

$$\Delta_\perp^{\mathrm{T}}\cdot J_f^{\mathrm{T}}\cdot f = \Delta_\perp^{\mathrm{T}}(M(q)\dot{\Delta}_\top + C(q,\dot{q})\Delta_\top)\nu_{\mathrm{L}} + \Delta_\perp^{\mathrm{T}} G(q) - \Delta_\perp^{\mathrm{T}}\tau \tag{11}$$

where the input $\tau = J_\tau^{\mathrm{T}}\cdot[\tau_\delta\ \ \tau_\varphi]^{\mathrm{T}}$ and

$$J_\tau = \begin{bmatrix} \mathrm{O}_{1\times 6} & 1 & \mathrm{O}_{1\times 2} & 0 & 0 \\ \mathrm{O}_{1\times 6} & 0 & \mathrm{O}_{1\times 2} & 1 & 1 \end{bmatrix}.$$

Similar to the case of Navier's table problem or Painleve paradox, the twelve-dimensional f cannot be identified by the nine equations in (11). Therefore, we define projected WFs onto the constrained space $\lambda = [\lambda_1\ \lambda_2\ \lambda_3\ \lambda_4\ \lambda_5\ \lambda_6\ \lambda_7\ \lambda_8\ \lambda_9]^{\mathrm{T}} = \Delta_\perp^{\mathrm{T}}(M(q)\dot{\Delta}_\top + C(q,\dot{q})\Delta_\top)\nu_{\mathrm{L}} + \Delta_\perp^{\mathrm{T}} G(q) - \Delta_\perp^{\mathrm{T}}\tau \in \Re^9$ which can be calculated with the known variables, and the proposed rollover prediction algorithm in Section V-A checks

the feasibility of the WFs required to uphold the no-rollover constraints using the zero moment point (ZMP) [17] calculated with λ instead of f. To predict the slip of each wheel using the friction cone model, the twelve-dimensional f is required to calculate the required friction coefficient, and we propose optimistic and pessimistic slip prediction algorithms in Section V-B using the relations $\Delta_{\perp}^{\mathrm{T}} \cdot J_f^{\mathrm{T}} \cdot f = \lambda$ which calculate the upper and lower bounds of the exact required friction coefficient calculated with f.

V. Proposed Planned Trajectory Classification Method

The rollover and slip prediction algorithms are proposed to check the feasibility of the rollover and slip prevention in this section. In practice, the rollover occurs if the ZMP [17] is at the outside of the supporting polygon (e.g., $y_{\mathrm{zmp}} > W_{\mathrm{l}}$ or $y_{\mathrm{zmp}} < -W_{\mathrm{r}}$), and the wheel slips if the friction coefficient of the road μ_{real} is less than the required friction coefficient (e.g., $\mu_{\mathrm{real}} < \sqrt{(f_i^x)^2 + (f_i^y)^2}/f_i^z$ for the i-th wheel) according to the friction cone model. In Section V-A, the rollover prediction algorithm is proposed by calculating the ZMP using λ. For the slip prediction, we propose optimistic and pessimistic slip prediction algorithms using the relations $\Delta_{\perp}^{\mathrm{T}} \cdot J_f^{\mathrm{T}} \cdot f = \lambda$ and the solution of the Navier's table problem [11] in Section V-B, and the PTCM is proposed in Section V-C using the results of the rollover and slip prediction algorithms.

A. Rollover Prediction Algorithm

When all the twelve-dimensional WFs are known, the x-axis moment in $\{\mathcal{B}\}$ at the zero moment point $O_{\mathrm{zmp}} = [x_{\mathrm{zmp}}\ y_{\mathrm{zmp}}\ z_{\mathrm{zmp}}]^{\mathrm{T}}$ is formulated as $M_x = (f_1^x \sin(\delta_1) + f_1^y \cos(\delta_1) + f_2^x \sin(\delta_2) + f_2^y \cos(\delta_2) + f_3^y + f_4^y) \cdot (H + r_w) + (f_1^z + f_3^z) \cdot (W_l - y_{\mathrm{zmp}}) - (f_2^z + f_4^z) \cdot (W_r + y_{\mathrm{zmp}}) = 0$, and y_{zmp} can be obtained as $y_{\mathrm{zmp}} = \{(\lambda_1 \sin(\delta_1) + \lambda_2 \sin(\delta_2) + \lambda_6) \cdot (H + r_w) + (T_f + T_r) \cdot (H + r_w) \cdot \lambda_5 \cos(\delta) + \lambda_8\} / \{(H + r_w) \cdot \lambda_5 \sin(\delta) + \lambda_7\}$ using the relations $\Delta_{\perp}^{\mathrm{T}} \cdot J_f^{\mathrm{T}} \cdot f = \lambda$. The proposed rollover prediction algorithm predicts the rollover if $y_{\mathrm{zmp}} > W_l$ or $y_{\mathrm{zmp}} < -W_r$.

B. Slip Prediction Algorithms

According to the friction cone model, the slip occurs when the horizontal force is larger than the maximum friction force, and the function of the maximum friction force with respect to the vertical force has a cone shape. The slope of the cone is called the friction coefficient, and the necessary and sufficient condition to prevent the slip of the i-th wheel can be expressed as $\mu_{\mathrm{real}} \geq \mu_i$ where $\mu_i = f_{\mathrm{hor},i}/f_{\mathrm{ver},i}$. The quantity μ_{real} is the friction coefficient of the road which can be estimated by the friction coefficient estimation algorithms [18], μ_i is the required friction coefficient to prevent the slip of the i-th wheel, and $f_{\mathrm{hor},i}$ and $f_{\mathrm{ver},i}$ are, respectively, the horizontal and vertical WFs of the i-th wheel, i.e., $f_{\mathrm{hor},i} = \sqrt{(f_i^x)^2 + (f_i^y)^2}$ and $f_{\mathrm{ver},i} = f_i^z$. Therefore, more than one wheel slips if $\mu_{\mathrm{real}} < \max_{i \in W} \mu_i(f) = \mu_{\max}$, and the quantity $\mu_{\max}$ cannot be exactly calculated for the 4-WMR, because the twelve-dimensional WFs are required to calculate $\mu_{\max}$. Therefore, we propose the optimistic and pessimistic slip prediction algorithms using the relations between f and λ that, respectively, predict the slip if the sufficient condition for the slip is satisfied and the sufficient condition for the no-slip is not satisfied, and we adopt the solution of the Navier's table problem [11] that distributes the vertical forces of the 4-leg tables. Under the high stiffness vertical suspension assumption $\epsilon_i \approx 0$ where ϵ_i is the displacement of the i-th suspension, the vertical forces should satisfy

$$f_1^z + f_4^z = f_2^z + f_3^z \tag{12}$$

if the distortion of the sprung mass is impossible as typical 4-WMRs according to the solution of the Navier's table problem in [11]. The proposed optimistic slip prediction algorithm defines the minimum required friction coefficient μ_c^{o}, and μ_c^{o} is the required friction coefficient when the largest required friction coefficient of the wheels is minimized. To calculate μ_c^{o}, an optimization problem is formulated as

$$\mu_c^{\mathrm{o}} = \min_f \max_{i \in W} \mu_i(f)$$

subject to

$$\mathrm{sgn}\,(f_i^y) = \mathrm{sgn}\,(\omega_z) \ \text{ for } {}^{\forall}i \in W \tag{13}$$

the relations $\Delta_{\perp}^{\mathrm{T}} \cdot J_f^{\mathrm{T}} \cdot f = \lambda$, and the equation in (12) where $\mu_j(f_{\min}) \geq \mu_i(f_{\min})$ for ${}^{\forall}i \in W$, $j = \arg\max_{i \in W} \mu_i(f)$, and $f_{\min} = \arg\min_f \mu_j(f)$ should be satisfied to avoid the change of the index j during the minimization. The function sgn(♣) is the sign function where (♣) is a scalar quantity. The constraint for the direction of the lateral force in (13) is derived by assuming that $L_{\mathrm{in}} > W_l$ or $L_{\mathrm{in}} < -W_r$ where this assumption should be satisfied for car-like 4-WMRs with steering angle limits (e.g., $|\delta_1| < \pi/2$ and $|\delta_2| < \pi/2$) according to the Ackermann steering geometry. If the minimum required friction coefficient μ_c^{o} is larger than μ_{real}, the proposed optimistic slip prediction algorithm predicts the slip. The proposed optimistic slip prediction algorithm is non-conservative, because the slip may occurs even though the sufficient condition of the slip $\mu_c^{\mathrm{o}} > \mu_{\mathrm{real}}$ is not satisfied, and a prediction algorithm using the sufficient condition of the no-slip (e.g., a pessimistic slip prediction algorithm) is required for the conservative no-slip prediction. The maximum required friction coefficient μ_c^{p} for the proposed pessimistic slip prediction algorithm can be calculated as

$$\mu_c^{\mathrm{p}} = \max_f \max_{i \in W} \mu_i(f)$$

subject to $\Delta_{\perp}^{\mathrm{T}} \cdot J_f^{\mathrm{T}} \cdot f = \lambda$ and the equations in (12) and (13), and the proposed pessimistic slip prediction algorithm predicts the no-slip if the sufficient condition for the no-slip $\mu_c^{\mathrm{p}} \leq \mu_{\mathrm{real}}$ is satisfied and the slip otherwise.

C. Planned Trajectory Classification

In this subsection, the planned trajectory is classified by using the proposed PTCM. Using the proposed rollover and slip prediction algorithms, the feasibility of the rollover and slip prevention can be checked, and the planned trajectory should be changed when the feasibility of the rollover and slip prevention are infeasible. The proposed PTCM classifies the planned trajectory into safe (e.g., no-rollover and no-slip) and unsafe trajectory

using the following conditional equation.

$$\begin{cases} \text{unsafe}, & \text{if } y_{\text{zmp}} > W_l,\ y_{\text{zmp}} < -W_r, \\ & \quad \mu_c^{\text{o}} > \mu_{\text{real}},\ or \mu_c^{\text{p}} > \mu_{\text{real}}, \\ \text{safe}, & \quad \text{otherwise}. \end{cases} \tag{14}$$

If the planned trajectory is classified as the unsafe trajectory, the trajectory should be modified for the safety, i.e., reducing the velocities of the 4-WMR near the infeasible part(s) of the planned trajectory.

VI. Simulation and Experiment

For the repeatability and the knowledge of the ground truth, the proposed PTCM is verified by simulations before outdoor experiments. For the simulations, a commercial software CarSim is used to evaluate the performance of the proposed PTCM, and more than thousand trajectories generated by CarSim are classified using the proposed PTCM. The CarSim provides the vertical tire forces, friction coefficient, slip ratio, and slip angle that can be used to calculate the ground truth of the rollover and slip times, and the prediction times of the rollover and slip are compared to the ground truth in Section VI-A. The true-positive probability, true-negative probability, and prediction accuracy are also provided in Section VI-A to evaluate the prediction performances of the proposed rollover and slip prediction algorithms. A 4-WMR is implemented for the outdoor experiments, and the trajectories of the implemented 4-WMR and friction coefficient of the road are, respectively, estimated using one of the recent visual inertial state estimation algorithm VINS-MONO [19] and the TFF-CKF [18]. The estimated trajectories are classified by the proposed PTCM, and the classification performances of the proposed PTCM is discussed in Section VI-B.

A. Simulation Results

To generate the trajectories using the CarSim, input torques, i.e., τ_d, are injected to the drive shaft of the differential gear, and all the gear ratios of the differential gear are set to one (e.g., $\tau_d = 2\tau_\varphi$). Each simulation is performed for eight seconds (e.g., $0 \le n \le 8$), and the input torque for the drive shaft τ_d is modeled as

$$\tau_d = \begin{cases} \tau_{d,1} \cdot \sin(2\pi \cdot \tau_{d,2} \cdot n) + \tau_{d,3} \cdot n, & \text{if n} \le 1, \\ \tau_{d,1} \cdot \sin(2\pi \cdot \tau_{d,2} \cdot n) + \tau_{d,3}, & \text{otherwise}, \end{cases}$$

where $\tau_{d,1}$, $\tau_{d,2}$, and $\tau_{d,3}$ are parameters to generate various trajectories. The steering angles of the front wheels are steered to follow the given trajectories which are generated for the practical double lane change scenario. The stiffnesses and damping coefficients of the suspensions are set as high as possible (e.g., 550 N/mm and 50 Ns/mm, respectively) to reduce the effect of the suspensions, and roads inclined in zero and five degrees are used for the simulations. For the rollover (or slip) prediction simulations, the trajectories are ignored if the slip (or rollover) is occurred before the rollover (or slip). The ground truth of the rollover and slip times (e.g., n_{roll} and n_{slip}) are defined as the minimum times that one of the vertical tire forces becomes less than or equal to zero and normalized slip σ_i is greater than one, respectively. The normalized slip is defined as $\sigma_i = \sqrt{(\sigma_{r,i}/\sigma_{rm,i})^2 + (\tan(\sigma_{a,i})/\tan(\sigma_{am,i}))^2}/\mu_{\text{real}}$ where $\sigma_{r,i}$, $\sigma_{a,i}$, $\sigma_{rm,i}$, and $\sigma_{am,i}$ are, respectively, the slip ratio, slip angle, maximum slip ratio point, and maximum slip angle point of the i-th wheel, and the prediction times of the rollover and slip using the proposed rollover and slip prediction algorithms are notated as $\hat{n}_{\text{roll}}$ and $\hat{n}_{\text{slip}}$, respectively.

Fig. 4. Trajectory examples for the rollover prediction(red: rollover, blue: no-rollover).

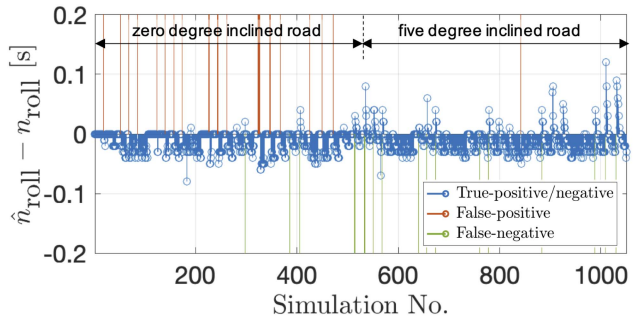

Fig. 5. CarSim simulation results of the proposed rollover prediction algorithm.

Fig. 6. Trajectory examples for the slip prediction (red: slip, blue: no-slip).

For the rollover prediction performance evaluation, $\tau_{d,1}$, $\tau_{d,2}$, and $\tau_{d,3}$ are selected as $\tau_{d,1} \in \{-500, -250, 0, 250, 500\}$, $\tau_{d,2} \in \{0.05, 0.075, 0.1, 0.125, 0.15\}$, and $\tau_{d,3} \in \{1450, 1500, 1550, \ldots, 2450\}$.

See Fig. 4 for trajectory examples for the rollover prediction. Fig. 5 shows the prediction time errors of the proposed rollover prediction algorithm (e.g., $\hat{n}_{\text{roll}} - n_{\text{roll}}$) for 1050 trajectories, and the true-positive and true-negative probabilities for the rollover prediction are, respectively, 89.9% and 97.7%. Among the 1050 trajectories, the 4-WMR drives on the zero degree inclined road for 525 trajectories and the five degree inclined road for another 525 trajectories as shown in Fig. 5. The number of the true-positive and true-negative simulations are added and then divided by the total number of simulations 1050 to calculate the prediction accuracy, and the prediction accuracy of the rollover is calculated as 95.7%. For the true-positive simulations, the mean of $|\hat{n}_{\text{roll}} - n_{\text{roll}}|$ is 0.0236 s.

The parameters $\tau_{d,1}$, $\tau_{d,2}$, and $\tau_{d,3}$ are selected as $\tau_{d,1} \in \{-500, -250, 0, 250, 500\}$, $\tau_{d,2} \in \{0.05, 0.075, 0.1, 0.125, 0.15\}$, and $\tau_{d,3} \in \{750, 800, 850, \ldots, 1750\}$ to generate trajectories for the slip prediction performance evaluation, and Fig. 6 shows trajectory examples for the slip prediction. Totally 1050 trajectories are simulated, yet only 829 trajectories are used for the slip prediction. The other 221 trajectories are ignored,

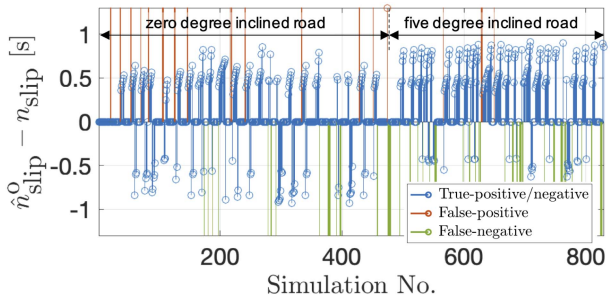

(a) Optimistic slip prediction results

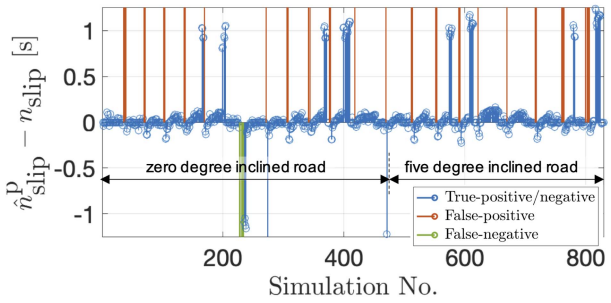

(b) Pessimistic slip prediction results

Fig. 7. CarSim simulation results of the proposed slip prediction algorithms.

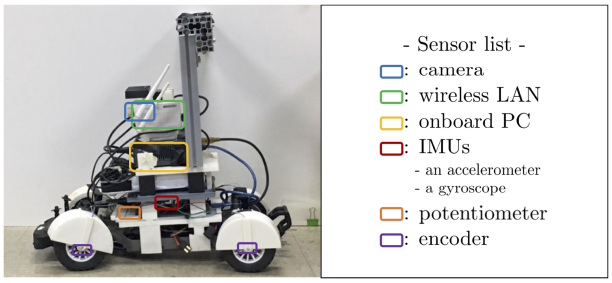

Fig. 8. Implemented 4-WMR with an onboard PC and sensors.

because the rollover is occurred before the slip. The 829 trajectories include 480 trajectories driving on the zero degree and 349 trajectories driving on the five degree inclined roads. The slip prediction time errors of the proposed optimistic and pessimistic slip prediction algorithms (e.g., $\hat{n}^{\mathrm{o}}_{\mathrm{slip}} - n_{\mathrm{slip}}$ and $\hat{n}^{\mathrm{p}}_{\mathrm{slip}} - n_{\mathrm{slip}}$) are, respectively, shown in Fig. 7(a) and (b). The true-positive probability, true-negative probability, and the accuracy of the optimistic slip prediction are, respectively, 83.2%, 91.5%, and 87.1%. The mean of $|\hat{n}^{\mathrm{o}}_{\mathrm{slip}} - n_{\mathrm{slip}}|$ is 0.5754 s for the true-positive simulations. The true-positive probability, true-negative probability, and the accuracy of the pessimistic slip prediction are, respectively, 98.6%, 79.0%, and 89.8%. The mean of $|\hat{n}^{\mathrm{p}}_{\mathrm{slip}} - n_{\mathrm{slip}}|$ is 0.1063 s for the true-positive simulations.

B. Experiment Results

A rearwheel driven 4-WMR with the Ackermann steering is implemented with an onboard PC and sensors as shown in Fig. 8. A traxxas Rally 1/10 RC car is modified to a rearwheel driven 4-WMR without the suspension, and an Intel NUC7i7BNH is

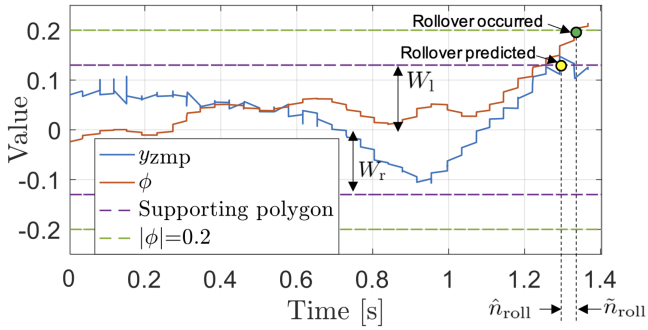

Fig. 9. Example of the rollover prediction results using the proposed rollover detection algorithm.

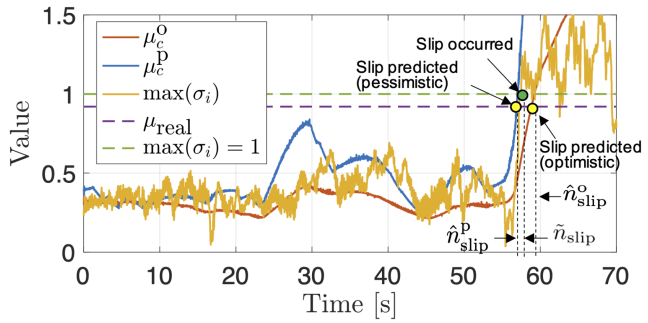

Fig. 10. Example of the slip prediction results using the proposed slip detection algorithms.

used as the onboard PC. To measure the acceleration and angular velocity of the body, IMU (an accelerometer and a gyroscope) included in the Advanced Navigation Spatial INS is placed at the CoG of the implemented 4-WMR, and a camera is installed above the IMU. Four RLS RM08 encoders are used to measure the wheel angular velocities, and a Piher PT-10 potentiometer is implemented to measure the steering angles of the front wheels. To obtain $\sigma_{rm,i}$ and $\sigma_{am,i}$ in the normalized slip σ_i, the magic formula tire model [20] is generated by using a tire model measuring equipment which is proposed in [18], and the estimated state and onboard sensor measurements are used to calculate $\sigma_{r,i}$ and $\sigma_{a,i}$ in σ_i. The VINS-MONO [19] is employed to estimate the trajectory using the measurements from the IMU and camera in 400 Hz, and the estimated trajectory is down-sampled to 100 Hz to be used as the planned trajectory for the proposed PTCM. Benchmark test results of the VINS-MONO can be found in [21].

To collect the estimated trajectories, the implemented WMR drives on a zero or ten degree inclined asphalt road. The average friction coefficient of the asphalt road is estimated as 0.92 using the TFF-CKF in [18]. Note that the friction coefficient of the typical asphalt roads is 0.8-1.0 [18]. The reference time of the rollover $\tilde{n}_{\mathrm{roll}}$ and slip $\tilde{n}_{\mathrm{slip}}$ are, respectively, defined as the minimum time that the magnitude of the estimated roll becomes greater than 11.46 ° (= 0.2 rad) and normalized slip σ_i becomes greater than one. Figs. 9 and 10 show rollover and slip prediction examples using the proposed rollover and slip prediction algorithms. With $\tilde{n}_{\mathrm{roll}}$ and $\tilde{n}_{\mathrm{slip}}$, the reference time $\tilde{n}$ is defined as $\tilde{n} = \min(\tilde{n}_{\mathrm{roll}}, \tilde{n}_{\mathrm{slip}})$ for each estimated trajectory, and the prediction time $\hat{n}^{(\star)}_{(*)}$ where $(*) \in \{\mathrm{roll}, \mathrm{slip}\}$ and $(\star) \in \{\mathrm{o}, \mathrm{p}\}$ is

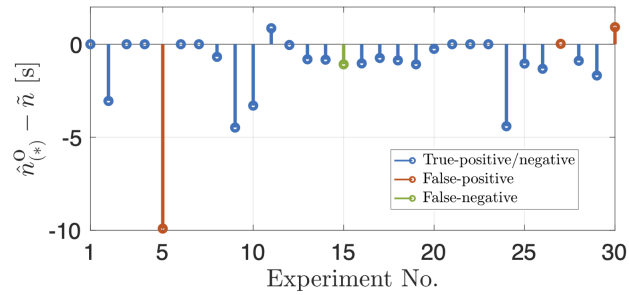

(a) w/ the proposed rollover and optimistic slip prediction algorithms

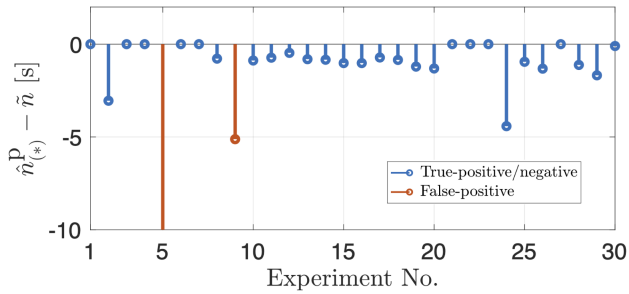

(b) w/ the proposed rollover and pessimistic slip prediction algorithms

Fig. 11. Experiment results of the proposed PTCM.

compared to $\tilde{n}$ to evaluate the classification performances of the proposed PTCM as shown in Fig. 11. For the thirty experiments in Fig. 11(a), the true-positive and the true-negative probabilities are, respectively, calculated as 95% and 70% using the proposed rollover and optimistic slip prediction algorithms. Using the proposed rollover and pessimistic slip prediction algorithms, the true-positive and the true-negative probabilities are, respectively, calculated as 100% and 80% for the thirty experiments as shown in Fig. 11(b). In Fig. 11, the prediction results that $\text{abs}(\hat{n}^{(\star)}_{(*)} - \tilde{n}) > 5$ is marked as the false-positive where $\text{abs}(\diamond)$ returns the absolute value of $(\diamond)$, because the rollover or slip is detected at the safe region of the trajectories.

VII. Conclusion

In this letter, a novel planned trajectory classification method (PTCM) is proposed to avoid the rollover and slip before executing the planned trajectory. The proposed PTCM calculates the WFs projected onto the constrained space and their relations with the WFs to prevent the rollover and slip using the decomposed dynamics of the 4-WMR, and the feasibility of the rollover and slip prevention is checked using the proposed rollover and slip prediction algorithms. The performance of the proposed PTCM is verified by simulations and outdoor experiments, and the proposed PTCM can be used to enhance the safety of the 4-WMRs with Ackermann steering and high-stiffness suspensions such as delivery and personal mobility WMRs.

References

[1] Grand View Research, "Intelligent transportation system market size, share & trends analysis report by type, by application (traffic management, road safety and security, freight management, Public Transport), By Region, And Segment Forecasts, 2022 - 2030," 2022. Accessed: Dec. 07, 2022. [Online]. Available: https://www.grandviewresearch.com/industry-analysis/intelligent-transportation-systems-industry

[2] J. Yoon, J.-H. Oh, J.-H. Park, S. Kim, and D. Lee, "Autonomous dynamic driving control of wheeled mobile robots," in *Proc. IEEE Int. Conf. Robot. Automat.*, 2014, pp. 5274–5279.

[3] W. Ding, L. Zhang, J. Chen, and S. Shen, "Safe trajectory generation for complex urban environments using spatio-temporal semantic corridor," *IEEE Robot. Automat. Lett.*, vol. 4, no. 3, pp. 2997–3004, Jul. 2019.

[4] W. Ding, L. Zhang, J. Chen, and S. Shen, "Epsilon: An efficient planning system for automated vehicles in highly interactive environments," *IEEE Trans. Robot.*, vol. 38, no. 2, pp. 1118–1138, Apr. 2022.

[5] C. C. Ward and K. Iagnemma, "A dynamic-model-based wheel slip detector for mobile robots on outdoor terrain," *IEEE Trans. Robot.*, vol. 24, no. 4, pp. 821–831, Aug. 2008.

[6] S. Lapapong, A. A. Brown, K. S. Swanson, and S. N. Brennan, "Zero-moment point determination of worst-case manoeuvres leading to vehicle wheel lift," *Veh. Syst. Dyn.*, vol. 50, no. sup1, pp. 191–214, Jan. 2012.

[7] C. Wang, Z. Wang, L. Zhang, D. Cao, and D. G. Dorrell, "A vehicle rollover evaluation system based on enabling state and parameter estimation," *IEEE Trans. Ind. Inform.*, vol. 17, no. 6, pp. 4003–4013, Jun. 2021.

[8] N. Seegmiller and A. Kelly, "Real-world validation of three tipover algorithms for mobile robots," in *Proc. Robot.: Sci. Syst.*, 2014, pp. 1–9.

[9] D. Lee, "Passive decomposition and control of nonholonomic mechanical systems," *IEEE Trans. Robot.*, vol. 26, no. 6, pp. 978–992, Dec. 2010.

[10] D. Lee and K. Y. Lui, "Passive configuration decomposition and passivity-based control of nonholonomic mechanical systems," *IEEE Trans. Robot.*, vol. 33, no. 2, pp. 281–297, Apr. 2017.

[11] S. Patnaik, D. Hopkins, and G. Halford, "Integrated force method solution to indeterminate structural mechanics problems," NASA, Washington, D.C., USA, Tech. Rep. NASA/TP-2004-207430, 2004.

[12] X. Xiong and A. D. Ames, "Sequential motion planning for bipedal somersault via flywheel slip and momentum transmission with task space control," in *Proc. IEEE/RSJ Int. Conf. Intell. Robots Syst.*, 2020, pp. 3510–3517.

[13] M. Kalakrishnan, J. Buchli, P. Pastor, M. Mistry, and S. Schaal, "Learning, planning, and control for quadruped locomotion over challenging terrain," *Int. J. Robot. Res.*, vol. 30, no. 2, pp. 236–258, 2011.

[14] Y. de Viragh, M. Bjelonic, C. D. Bellicoso, F. Jenelten, and M. Hutter, "Trajectory optimization for wheeled-legged quadrupedal robots using linearized ZMP constraints," *IEEE Robot. Automat. Lett.*, vol. 4, no. 2, pp. 1633–1640, Apr. 2019.

[15] L. Righetti, J. Buchli, M. Mistry, M. Kalakrishnan, and S. Schaal, "Optimal distribution of contact forces with inverse-dynamics control," *Int. J. Robot. Res.*, vol. 32, no. 3, pp. 280–298, 2013.

[16] Y. Shi, Y. Huang, and Y. Chen, "Trajectory planning of autonomous trucks for collision avoidance with rollover prevention," *IEEE Trans. Intell, Transp. Syst.*, vol. 23, no. 7, pp. 8930–8939, Jul. 2022.

[17] S. Kajita et al., "Biped walking pattern generation by using preview control of zero-moment point," in *Proc. IEEE Int. Conf. Robot. Automat.*, 2003, pp. 1620–1626.

[18] S.-Y. Jeon, R. Chung, and D. Lee, "Tire force estimation of dynamic wheeled mobile robots using tire-model based constrained Kalman filtering," in *Proc. IEEE/RSJ Int. Conf. Intell. Robots Syst.*, 2018, pp. 270–2477.

[19] T. Qin, P. Li, and S. Shen, "VINS-Mono: A robust and versatile monocular visual-inertial state estimator," *IEEE Trans. Robot.*, vol. 34, no. 4, pp. 1004–1020, Aug. 2018.

[20] H. B. Pacejka and I. Besselink, *Tire and vehicle dynamics*, 3rd ed. London, U.K.: Butterworth-Heinemann, 2012.

[21] J. Delmerico and D. Scaramuzza, "A benchmark comparison of monocular visual-inertial odometry algorithms for flying robots," in *Proc. IEEE Int. Conf. Robot. Automat.*, 2018, pp. 2502–2509.